Quest for the source of Meteosat anomalies

A.J.Coates, A.D.Johnstone, D.J.Rodgers
Mullard Space Science Laboratory, University College London,
Holmbury St Mary, Dorking, Surrey RH5 6NT, UK

G.L.Wrenn
Space Department, Royal Aerospace Establishment,
Farnborough, Hants GU14 6TD, UK

Abstract

Three ESA Meteosat geostationary satellites have suffered from a series of anomalies which disturb routine operations; most commonly, the scan of the radiometer has stopped or jumped requiring a reset command to be sent.

Experience with Meteosat-F1 launched in 1977 (Robbins, 1979) prompted the installation of an AFGL electron spectrometer (50eV-20keV) on Meteosat-F2, in an attempt to demonstrate a direct link between the anomalies and surface charging. Data spanning August 1981 to March 1987 have provided interesting evidence for differential charging (Wrenn and Johnstone, 1987) and permit the establishment of an empirical model of charging fluxes through a solar cycle. However, the reported anomalies do not fit the pattern for surface charging effects and no real link was found. Deep dielectric charging has now become the most likely explanation and consequently Meteosat-P2, launched in June 1988, carries a LANL monitor of 43-300 keV electrons.

The Meteosat anomaly chronicle is the result of reliable recording procedures at ESOC and it represents a unique data base for an important class of ESD effects which occur at Geosynchronous orbit. This paper gives some preliminary results from Meteosat P2 and attemptes to assess their relevance within the context of earlier conclusions from the Meteosat-F2 studies.

INTRODUCTION

Since Meteosat-F1 suffered many operational anomalies it was decided to include a spacecraft charging monitor on F2 to see whether the anomalies were related to spacecraft surface charging. While that experiment certainly showed strong evidence of charging on F2 there was no correlation with the occurence of unexplained anomalies, which were also present on F2. The decision was then made to investigate the higher energy range of electrons associated with deep dielectric charging. Thus SEM-2 was commissioned to study the 30-300keV range of electrons.

The sensor unit was provided by Los Alamos National Laboratory, USA as a spare Lo-E sensor [Aiello et al, 1975] from other programmes, to the Mullard Space Science Laboratory of University College London (MSSL) which provided the power supplies, data processing unit and interface to the Meteosat spacecraft. MSSL was further responsible for integration, testing and calibration of the instrument, and delivery of the instrument to the spacecraft. MSSL also provided a memory upset monitor (MUM) in this instrument, as requested by ESA.

This paper describes briefly the history of the F1 and F2 studies, in particular the role of spacecraft charging in generating the anomalies and the possibility of deep dielectric charging as an explanation. We then go on to a description of the SEM-2 instrument, and the conversion of the observed counts to physical units. Typical natural events in the spacecraft environment as seen by SEM-2 are shown. The correlation of the energetic electron fluxes to the occurence of anomalies, which on P2 occur at a rate which is about four times that of F2, are the major results. As data have accumulated we have been able to show a striking correlation between the energetic electron fluxes and the spacecraft anomalies. For the first time it appears that the measurements provide a good indication of anomalies.

1 Meteosat operational anomalies and spacecraft charging

1.1 Meteosat-F1

When Meteosat-F1 was launched in 1977 many operational anomalies occurred (about 150 in 3 years) for which there was no immediate explanation. However, their occurrence was related to geophysical factors outside the normal realm of spacecraft engineering, namely that they were more likely when there was strong geomagnetic activity and they exhibited a tendency to occur at certain times of day [Robbins, 1979]. It had recently been discovered then that geosynchronous spacecraft could charge up to many thousands of Volts [deForest, 1972] in the ambient plasma so it was natural to attribute the anomalies to charging, or more precisely to differential charging. Unless the complete outer surface of the spacecraft is conductive and

electrically connected, it is normal for different parts of the spacecraft to charge to different voltages. At times, adjacent surfaces can be more than a thousand volts apart. This in turn leads to arcing between the surfaces and results in large electrical transients in the spacecraft harness. After the problems were encountered by Meteosat-F1 a series of laboratory tests was carried out which demonstrated that arcing occurred if the spacecraft was illuminated by an electron beam, and that electrical transients could induce anomalous behaviour. It was not possible to simulate in-orbit conditions completely and thus it was not possible to establish the causal chain completely.

1.2 Meteosat-F2

Before the second spacecraft Meteosat-F2 was launched some changes were made to reduce the susceptibility to differential charging, namely grounding of thermal shields and hardening of some critical electrical interfaces, and to include two charging monitors to complete the link between the anomalies and spacecraft charging. One of the monitors was designed to detect arcing transients on a short antenna within the spacecraft. In flight no such events were detected, but it is not known whether the instrument was sensitive enough, or whether it was not operating correctly or whether there were no significant transients. Therefore we can say no more about it. The second monitor measured the ambient plasma electrons in the energy range 50eV to 20KeV and therefore could measure the charging current directly. Not only that but it was anticipated that in the event of spacecraft charging the energy spectrum would be modified in a manner which would allow the spacecraft potential to be measured. Briefly, the objective of the instrument was to see if the anomalies occurred when the spacecraft was charged. The results of this investigation have been published in a number of reports [Johnstone et al, 1985, Wrenn and Johnstone, 1987]. Although no direct link between differential charging and anomalies was found there were several interesting and significant (for this problem) findings which we summarize here.

1. Two types of differential charging were observed. One type occurred during eclipses and had been expected. The second type called a "barrier event", only occurred when the radiometer mirror was completely in shadow and was therefore probably because the mirror was charging up. The two types are illustrated in Figures 1 and 2 and explained in the figure captions.

2. A charging index based on an estimate of the net electron flux to the spacecraft (incident electrons minus secondary emitted electrons) was 95 percent successful in predicting whether the spacecraft would charge up in any particular eclipse.

3. There was an indication in the electron spectrum during eclipse charging that the voltages in differential charging were limited by discharging currents of secondary electrons from one part of the spacecraft to another.

4. Only one anomaly, in more than 100, occurred at any time near an observable differential charging event. In all cases there was no evidence that the spacecraft was charged to more than a few volts.

5. The anomalies attributed for lack of a better cause to arcing did, as before on Meteosat-F1, show a dependence on geophysical parameters, ie local time, solar aspect angle and geomagnetic activity [see Figure 3].

6. When separated into four types of anomaly the solar aspect angle, and local time dependence was different for all four groups.

7. The most common type of anomaly, the radiometer stoppage or position jump was most common at the equinox and was associated with a period of sustained high geomagnetic activity.

The conclusions of the analysis were that the anomalies were not the result of differential charging but that they were caused by some external geophysical effect. The four types of anomaly were caused by four different mechanisms.

Frezet et al [1989] have made an analysis of the charging of Meteosat with the NASCAP charging analysis code. They find that the differential voltages developed are greater at equinox and suggest that this is the explanation for the occurrence of radiometer anomalies at this time. The charging levels they obtain are many thousands of volts. However the only differential charging of the radiometer is observed away from equinox, when the radiometer mirror is totally in shadow. Also when anomalies occur there is no evidence of any charging. Finally Frezet et al only developed such a charging scenario when extreme plasma conditions are used and such extreme conditions were not observed by the monitors on Meteosat-F2 itself.

We were left with the situation that we still do not know what caused the anomalies on Meteosat-F1 or F2. Spacecraft surface charging, or differential charging, appears to be ruled out. In their final report Johnstone et al [1985] suggested that it might be caused by penetrating electrons producing deep dielectric charging. This was partly based on the observation that a sustained period of high geomagnetic activity was required to develop the effect, and that the trapped energetic electrons are known to be slower to respond to geomagnetic activity than the plasma at energies of less than 20KeV. Therefore it was suggested that the third Meteosat flight should carry a detector of more energetic electrons. Accordingly it was decided to include in the payload the SEM-2 detector which measures the energy and angular distribution of electrons in the energy range 30KeV to 300KeV.

The behaviour of electrons above 30keV at Geosynchronous orbit has been studied by the Los Alamos group [Baker et al, 1981]. In Figure 4 the average fluxes for the whole of 1977 and 1978 are compared to the particles' range in aluminium as calculated by the SHIELDOSE program: this shows that higher energy particles can penetrate appreciable distances before being stopped. To penetrate 0.5mm into polythene, an electron requires an energy of 200KeV (see Figure 5 from Powers et al. [1981]). Deep dielectric charging, where penetrating electron fluxes may cause buildup of charge and eventual breakdown in insulators, has been postulated as the reason for anomalies on other spacecraft [eg Baker et al, 1986].

2 Instrumentation

The measurement of electrons above 30 keV implies a different type of sensor to the F2 instrument, which consisted of two electrostatic energy analyser/channeltron combinations, giving differential energy measurements. The standard technique for tens to hundreds of keV particles has become the surface barrier solid-state detector [eg Aiello et al, 1975]. Using electronic thresholds this technique also gives differential energy measurements.

SEM-2 contains five surface barrier detector-collimator systems, arranged to accept particles from 5 different angular ranges. The 5 ranges are of spacecraft polar angle: azimuthal angle measurements are achieved by timing. Each of the detectors has 5 different energy ranges; the energy acceptances were found by calibration at the Goddard spaceflight center and are as follows:

Energy level	E_{min} (keV)
E5	42.9
E4	59.4
E3	90.7
E2	134.9
E1	201.8

Table 1: Lower level discriminator settings for SEM-2

Full details of the operation of the instrument are given in the final report to ESA (Coates et al, 1989). Here we restrict ourselves to a description of the information transmitted.

A transmission list is accumulated in 4 formats, approx 100 seconds. A complete experiment cycle takes 500 or 600 seconds since one polar angle is sampled in each 4-format cycle. The raw parameters received on the ground are as follows, every 100 seconds.

- A 5-point energy spectrum, compressed counts E1-E5, for a particular polar angle, summed over azimuth.
- A 6-point azimuth array, compressed counts A1-A6, for a particular polar angle, summed over energy.
- Overflow information as appropriate for each of the above bins.
- Timing information to relate azimuth to spin phase.
- Synchronisation information for data checking.
- MUM parameters on SEU and latch-up.

Counts are converted to flux and plotted. The principal result of the data processing was the provision of summary plots of the data from SEM-2. It is essential that users of the SEM-2 data be able to tell from the plots alone, the general behaviour of the plasma environment at all times and be able to identify times of particular interest. To enable this, the plots contain parameters that summarise the data, parameters that interpret the data further and associated parameters for comparison. This led to the choice of eight panels of data presented on a single page with one page per day; an example is shown in Figure 6. These panels are: Total Flux; Flux; Spectral Index; Polar Flow; Azimuthal Flow; Anisotropy Index and axis of symmetry; Kp; MUM and Latch-up.

2.1 Total Flux

Total flux of electrons within the energy range of the detector (42.9-300keV) and summed over all polar and azimuthal bins.

2.2 Flux

This is the Flux (expressed as a grey scale level) in the 5 energy bands of the analyser, from 43 to 300KeV. These energy bands are: 42.9 to 59.4KeV, 59.4 to 90.7KeV, 90.7 to 134.9KeV, 134.9 to 201.8KeV, 201.8 to 300(nominal)KeV. These data are summed over all polar and azimuthal angle bins.

The analyser returns integral measurements of counts versus energy. Counts are measured as the energy cut-off or threshold of the instrument is progressively raised. To calculate the counts in one energy band, the counts measured with the cut-off at the top and bottom of that band are subtracted.

2.3 Spectral Index

This index determines the 'hardness', or shape of the energy spectrum. This is generally negative because, except in extraordinary cases, there are less particles at high energy than at low energy. The index is simply the slope of the log of the energy spectrum.

2.4 Polar Flow

This is the flux (expressed as a grey scale) in the 5 polar angle sectors of the analyser. These sectors look in the polar directions 30°, 60°, 90°, 120° and 150° to the spacecraft spin axis. The spacecraft spin axis is to a good approximation parallel to the Earth's spin axis. The angle bins cover a nominal ±5°.

2.5 Azimuthal Flow

This is the flux (expressed as a grey scale) in the 6 azimuthal angle sectors of the analyser. These sectors cover the angles 0° to 60°, 60° to 120°, 120° to 180° , 180° to 240°, 240° to 300° and 300° to 360°, in spacecraft coordinates. Note that at 0° the analyser looks towards the sun.

2.6 Anisotropy Index and axis of symmetry

The anisotropy index describes the angular shape of the plasma distribution relative to its axis of symmetry, shown as theta and phi. A trapped particle distribution is a 'pancaked' i.e. enhanced perpendicular to the magnetic field compared to along it. Where plasma is newly injected it tends to lie along the field line in a 'cigar-shaped' distribution. The index is positive for pancaked distributions and negative for cigar-shaped distributions. The anisotropy index is calculated [using techniques adapted from Sanderson and Page, 1974, Sanderson and Hynds, 1977, Higbie and Moomey, 1977] by fitting the data to a set of spherical harmonics. Since we believe that the magnetic field organizes the plasma, then the axis of symmetry represents the magnetic field direction. However, it does not distinguish between positive and negative field directions.

2.7 Kp and Kp(τ)

Kp is an index of planetary magnetospheric activity for the whole of Earth, in a three hour period. In the monthly plots, Kp(τ) is plotted. This is a weighted average of successive Kp values and was devised by Wrenn [1987]. Many magnetospheric processes are more dependent on the general level of magnetospheric activity in the recent past than on the present level. Wrenn showed that anomalies on Meteosat-F2

was better correlated with an appropriately time-averaged activity index than with the real-time index.

2.8 MUM

The Memory Upset Monitor results are displayed as lines in the bottom panel. These display the number of 'single-event upsets' i.e. errors found in a known memory pattern, in the 4 memory zones of the test RAM. A test pattern is seen in the plot when the instrument is first powered on. A fifth line in this plot shows the occurrence of 'Latch-ups' where the test RAM attempts to draw excessive current. This line can take only values 1 – Latch-up and 0 – no latch-up.

3 Typical events

To illustrate the envoronment at Geosynchronous orbit as seen by Meteosat-P2 SEM-2 we include some data examples.

27th June 88 (Figure 6): On the dayside, eg at 1300Z, a "pancake" distribution is seen in the polar angle plot where fluxes are peaked at the equator: this is typical for a trapped electron distribution diffusing into the loss cone. At approximately 0200Z there is a typical isolated, injection event which shows some important features. First the total flux drops by two orders of magnitude, relatively slowly. Then it increases sharply to a level greater than before. Finally it decreases slowly to the initial level.

In Figure 7 we have looked at the results from 4 satellites simultaneously to the injection in Figure 6. Local time around the Earth is seen in the small inset diagram; spacecraft 1 and 2 (Meteosat) see the injection, while 3 and 4 show velocity dispersion with higher energy electrons arriving first.

The monthly summary example in Figure 8 shows the wider view of the dramatic events during March 1989. The spacecraft was outside the magnetopause for significant times on March 13 since the magnetosphere was severely compressed at that time.

4 Meteosat anomaly correlations

When comparing the occurrence of anomalies with the results from SEM-2 on a monthly basis it soon became apparent that anomalies, particularly radiometer anomalies, nearly always occurred when the flux of energetic electrons was high. The problem then becomes to verify such an association statistically and then to try and determine a causal link. While we have been able to achieve the former,

the latter is still some way from a satisfactory conclusion. In other words there is no doubt that anomalies and high energetic electron fluxes are linked but we do not yet know if the energetic electrons cause anomalies and if they do, how they do. Alternatively the high electron fluxes may themselves be the consequence of another agent which is the actual cause of the anomalies.

A plot of the anomalies we have used in this study is given in Figure 9, where we have organized the anomalies as follows:

RPJ Radiometer position jump
RDS Radiometer stoppage
RGC Radiometer gain change
BAT Battery anomaly
SIC SIC anomaly
OTH Other anomaly

RDS is by far the most frequent type of anomaly.

First we establish that the radiometer anomalies show the same systematic behaviour as on the previous Meteosat flight models. Figure 9 shows the local time and annual distribution for the 76 unexplained anomalies seen in the first year. They are essentially identical with distributions obtained for F2. In local time the peak occurrence is in the period 02 to 05 local time but there is a non-negligible rate of occurrence throughout the day. This distribution is reminiscent of the distribution of a type of charging event on Meteosat-F2 which were called barrier events [Johnstone et al, 1985]. However none of the Meteosat-F2 anomalies was concurrent with a barrier event. Anomalies are, as with F2, are most likely at the equinoxes and least likely at the solstices. This demonstrates once again essentially a dependence on solar aspect angle. The main conclusion we wish to draw from this diagram is that the radiometer anomalies are caused by the same mechanism as on Meteosat-F2. It is interesting to note that the anomaly rate is approximately 4 times that of F2, which suffered 80 anomalies in 4 years.

In the next series of plots the statistics of the average daily flux is examined. Figure 10 is a histogram of the number of days in the year a particular value of the daily average flux was recorded. For example the column labelled 7 contains number of days the average fluxes were in the range 7000 to 7999. Thus this graph if normalized would show the probability that the average flux has a particular value. It could be used for example to calculate the amount of radiation a geosynchronous satellite would encounter. Figure 11 shows the yearly total number of anomalies which occurred on days with that average daily flux. Compared with the distribution of Figure 10 it is clearly strongly biased towards the higher fluxes. By dividing the distribution of Figure 11 by that in Figure 10 we calculate the average number of anomalies in a day if the average flux has the given value. This produces the very striking distribution shown in Figure 12. Once the flux exceeds 19000 the average daily rate is greater than one. This can be interpreted as the probability of an

anomaly in given flux conditions. It is the first time we have achieved a connection between a characteristic of the plasma environment and the occurrence of anomalies. No such connection was found between the low energy plasma (E < 20 KeV) environment and anomalies on Meteosat-F2.

This does not yet establish a causal connection because the high fluxes could be caused by the same unknown phenomenon which causes the anomaly. What about the annual variation in the occurrence? This could arise because the energetic electron fluxes have a similar annual variation. In Figure 13 the mean monthly flux (dotted line) is plotted with the monthly number of anomalies. Both show a peak in March and April which were two of the most active months magnetically for a long time. In Sept and Oct where the anomaly rate peaks the monthly mean flux actually has its minimum value for the year. This suggests that there are at least two independent factors responsible for radiometer anomalies; one is associated with high fluxes of energetic electrons fluxes, and the other with the solar aspect angle.

It is possible that there is a third factor, which we see in the form of the local time variation of anomalies. This is likely however to be linked to a local time variation in the energetic electron fluxes. We have not been able to test this hypothesis yet because of the need to develop some specialised software to access this aspect of the data.

These results give us a positive result on the cause of anomalies for the first time. It is difficult to achieve a better level of proof without having a clearer idea of the mechanism which will allow us to develop a physical model which can be directly tested. An attempt to do this based on deep dielectric charging will form the next stage of our investigation.

The interaction between Meteosat and the environment is clearly a very complex one which we do not yet understand. Although spacecraft charging is significant, and needs to be minimized as we have now learned, there are other things going on for which we have not yet found the appropriate ameliorative methods.

Clearly the investigation should continue. Ideas of such effects as deep dielectric charging are still vague and need to be sharpened. This may require laboratory testing to try to replicate the phenomena, and the development of physical models which can be tested against the observations. There is also still a need to observe in more detail the interaction of a spacecraft with its environment and over a wide range of energies.

5 Summary of results

- Unexplained anomalies on Meteosat-P2 have continued at a rate about 4 times higher than that observed on F2. The P2 and F2 anomalies show a similar local time and seasonal dependance.

- The anomalies show a good correlation with electron fluxes in the range 43-300keV. This is the first time that a correlation of anomalies has been demonstrated with the Meteosat in-situ environment monitor data - the charging instrument on F2 saw charging events but they did not correlate with anomalies. Taken on its own the P2 correlation would confirm deep dielectric charging as a possible mechanism.
- However the seasonal dependence of anomalies, which strongly peak at equinox, show that at least one additional process is at work.
- We still maintain that spacecraft charging cannot explain the observed Meteosat anomalies, although it should still be minimised to avoid others.

6 Further study

Future study will be pursued on the following items:

- Processing of further SEM-2 data (already underway at MSSL).
- An explanation should be sought for the seasonal variation of anomalies on Meteosat.
- Further study is needed on the deep dielectric charging mechanism.
- Further effort should be put into calculating dose rates and penetration depths from the SEM-2 data.
- Further instruments should be included on future spacecraft, not only Meteosat, to look at both charging and deep dielectric effects. For the Meteosat series, higher energy electrons measurements extending up to 1MeV are encouraged to study the deep dielectric charging in more detail.

ACKNOWLEDGEMENTS

Most of this work was performed as part of ESA contract 7879/88/F/TB. The SEM-2 sensor head was provided by Los Alamos National laboratory, thanks are due to R.Belian and W.Aiello. T.A.Fritz made a new unit available when launch delays caused calibration and noise problems; he also provided the Los Alamos data shown in Figure 7. Calibration was done at NASA-Goddard Spaceflight Center: S.Brown and C.Smith are gratefully acknowledged. The interest, help and patience of the ESA Meteosat project team, principally J.Aasted, was much appreciated particularly regarding installation of the new sensor head.

7 References

Aiello, W.P., Belian, R.D., Conner, J.P., Higbie, P.R., Martin, W.B. & Singer, S., "An energetic particle detector for a synchronous satellite", *IEEE Trans Nucl Sci*, **NS-22**, 575, 1975.

Baker, D.N., Belian, R.D., Higbie, P.R., Klebsbadel, R.W. and Blake, J.B., "Deep dielectric charging effects due to high energy electrons in Earth's outer magnetosphere", submitted to *J.Electrostatics*, 1986.

Baker, D.N., Higbie, P.R., Belian, R.D., Aiello, W.P., Hones, E.W.,Jr., Tech, E.R., Halbig, M.F., Payne, J.B., Robinson,R. and Kedge, S., "The Los Alamos Geostationary Orbit Synoptic Data Set: a compilation of energetic particle data", *Los Alamos report LA-8843*, 1981.

Coates, A.J., Johnstone, A.D., Rodgers, D J and Huckle, H.E., "SEM-2 ,data processing 22 June 1988 to 30 June 1989", report on ESA contract 7879/88/F/TB, 1989.

DeForest, S.E., "Spacecraft charging at synchronous orbit", *J.Geophys.Res.*, **77**, p651, 1972.

Frezet, M., Daly, E.J., Granger, J.P and Hamelin, J., "Assessment of electrostatic charging of satellites in the geostationary environment", ESA Journal, **13**, 89-117, 1989.

Higbie P.R. and Moomey W.R. "Pitch Angle Measurements from Satellites Using Particle Telescopes with Multiple View Directions", *Nucl. Instrum Methods*, **146** p.439, 1977.

Johnstone A.D., Wrenn G.L., Huckle H.E. and Scott R.F. "Meteosat-F2 Spacecraft Charging Monitors", Final Report ESA contracts 4715/81/F/CG, 5911/84/F/CG, 1985.

Powers W.L., Adams B.F. and Inouye G.T. "Electron Penetration of Spacecraft Thermal Insulation", Spacecraft Charging Technology 1980, *AFGL-TR-81-0270*, p.86, 1981. ADA114426

Robbins,A., "Meteosat spacecraft charging investigations", final report, ESA contract 3561/78F/CG/SC, 1979.

Sanderson T.R. and Hynds R.J. "Multiple Telescope Measurements of Particle Anisotropies in Space", *Planet. Space Sci.*, **25** p.799, 1977.

Sanderson T.R. and Page D.E. "Spherical Harmonic Analysis of Satellite Anisotropy Measurements", *Nucl. Instrum. Methods*, **119**, p.177, 1974.

Wrenn G.L., "Time-Weighted Accumulations ap(τ) and Kp(τ)", *J. Geophys. Res.*, **92**, no. A9, p.10125, 1987.

Wrenn, G.L. and Johnstone, A.D., "Evidence for differential charging on Meteosat-2", *J.Electrostatics*, **20**, 59-84, 1987.

8 Figure captions

Figure 1 - An eclipse charging event seen by the F2 experiment. From the change in the energy spectrum it is inferred that the potential of the whole satellite went 5kV negative relative to space in this eclipse. The rising peak is due to differential charging of another part of the spacecraft at an even more negative potential (up to 600V more negative). [from Johnstone et al, 1985].

Figure 2 - Example of a "barrier event" on F2. This is where part of the spacecraft, electrically isolated from the rest, is shadowed and charges negatively as the whole spacecraft does in eclipse. High potential differences between adjacent parts of the spacecraft may then result in arcing. The low energy electrons observed in the event are due to reflection by the potential barrier of photo- and secondary electrons back to the spacecraft. While these events were correlated with radiometer mirror shadowing they were not correlated with observed anomalies. [from Johnstone et al, 1985].

Figure 3 - Distribution of F2 anomalies in local time and season [from Wrenn, 1989].

Figure 4 - Average electron flux spectra averaged over the 2 years 1977 and 1978. 90% of the samples are below the top curve and above the bottom curve. Mean electron ranges are also plotted. [fluxes from Baker et al, 1981, range from SHIELDOSE code developed by Seltzer (NBS 1116)]

Figure 5 - Electron range in polyethylene [from Powers et al, 1981]

Figure 6 - Daily plot for 27 June 88 showing an injection event at 0220Z.

Figure 7 - Energetic electron measurements from various positions at Geosynchronous orbit around the earth (see inset), showing the 27 June injection on spacecraft 1 and 2 (Meteosat) and velocity dispersion effects on 3 and 4. 1,3,4 are US spacecraft, those data courtesy LANL.

Figure 8 - Monthly plot for March 89

Figure 9 - All P2 anomalies as a function of local time and date

Figure 10 - Number of days with given average flux (thousands of flux units)

Figure 11 - Anomalies as a function of daily flux

Figure 12 - Average daily anomaly rate (anomaly probability) as a function of daily flux

Figure 13 - Anomalies (solid line) and monthly mean flux (dotted line for different months

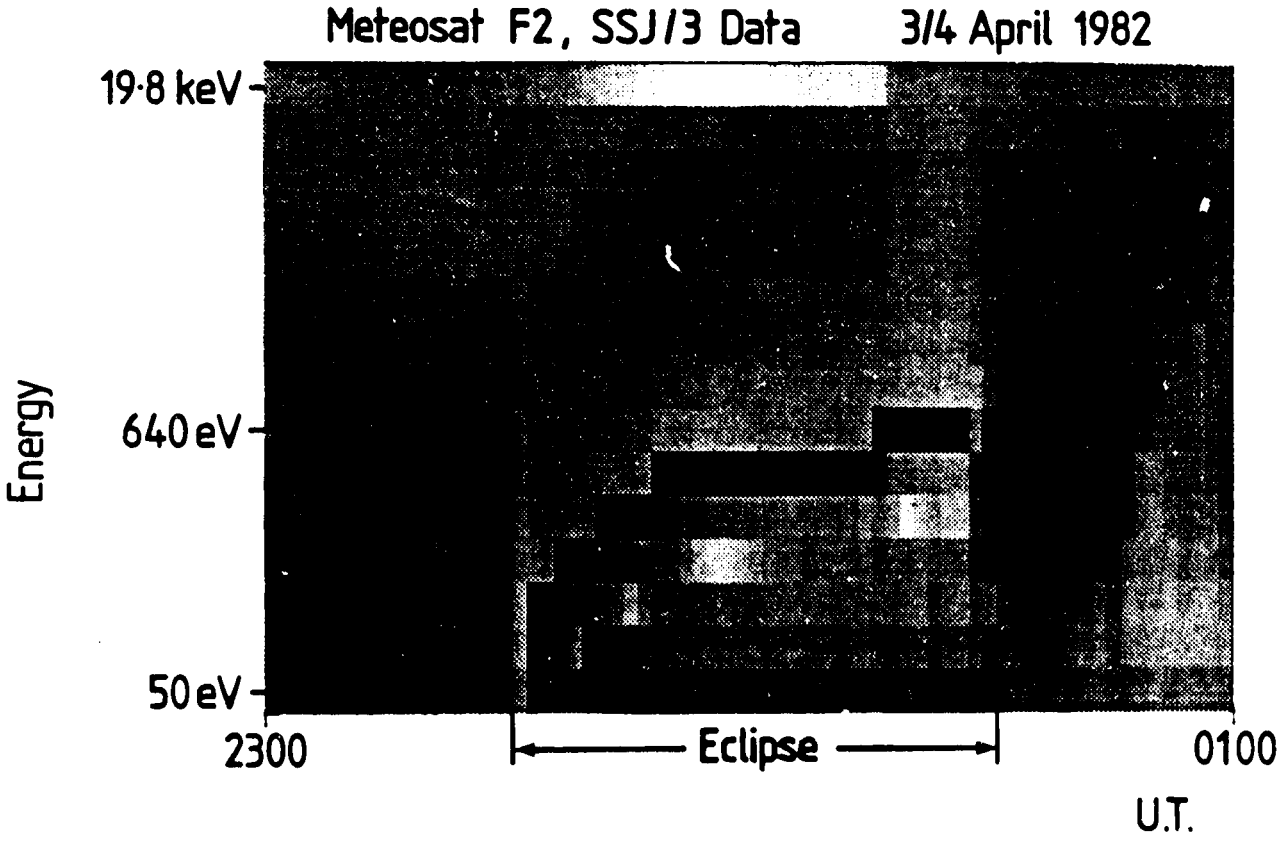
Meteosat F2, SSJ/3 Data 3/4 April 1982
19·8 keV
640 eV
50 eV
Energy
2300
Eclipse
0100
U.T.

Figure 1

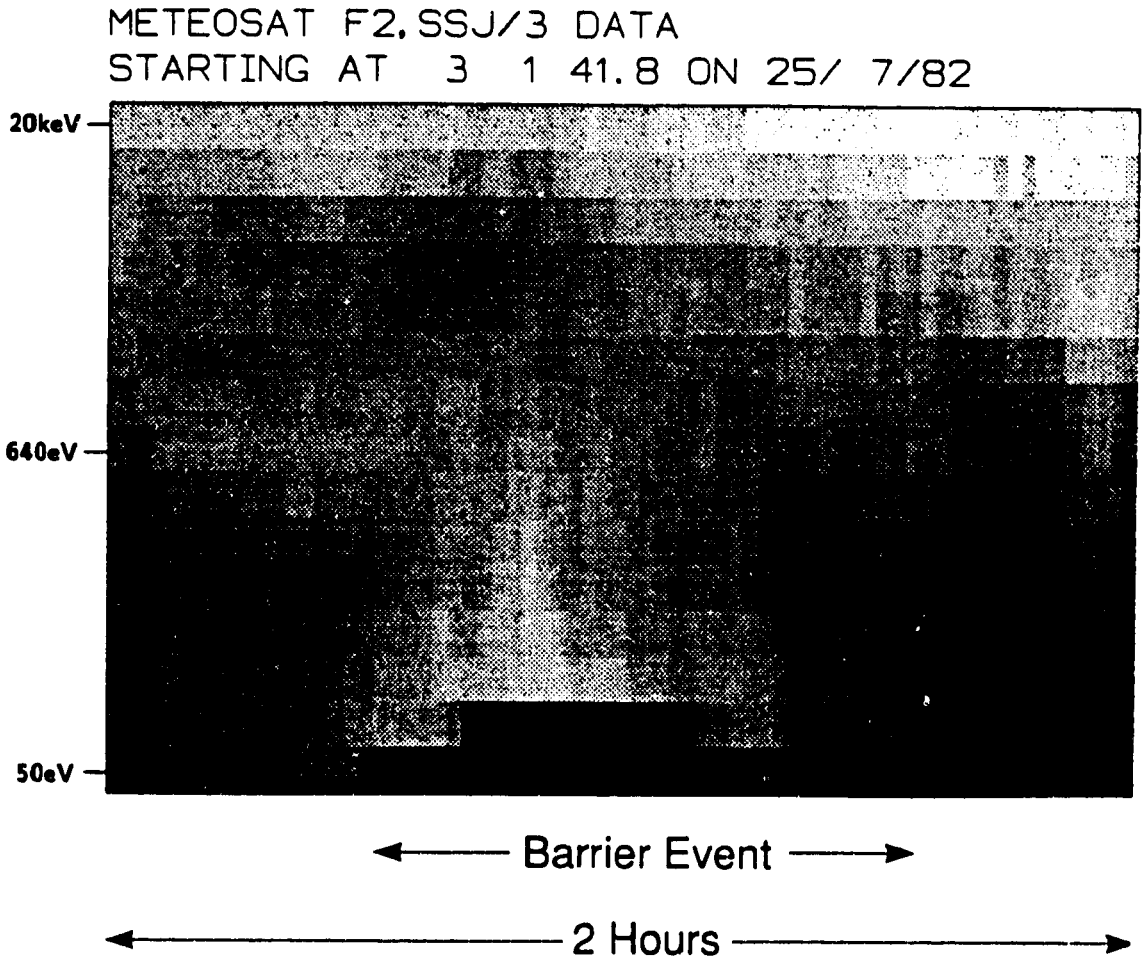
METEOSAT F2, SSJ/3 DATA
STARTING AT 3 1 41.8 ON 25/ 7/82
20keV
640eV
50eV
Barrier Event
2 Hours

Figure 2

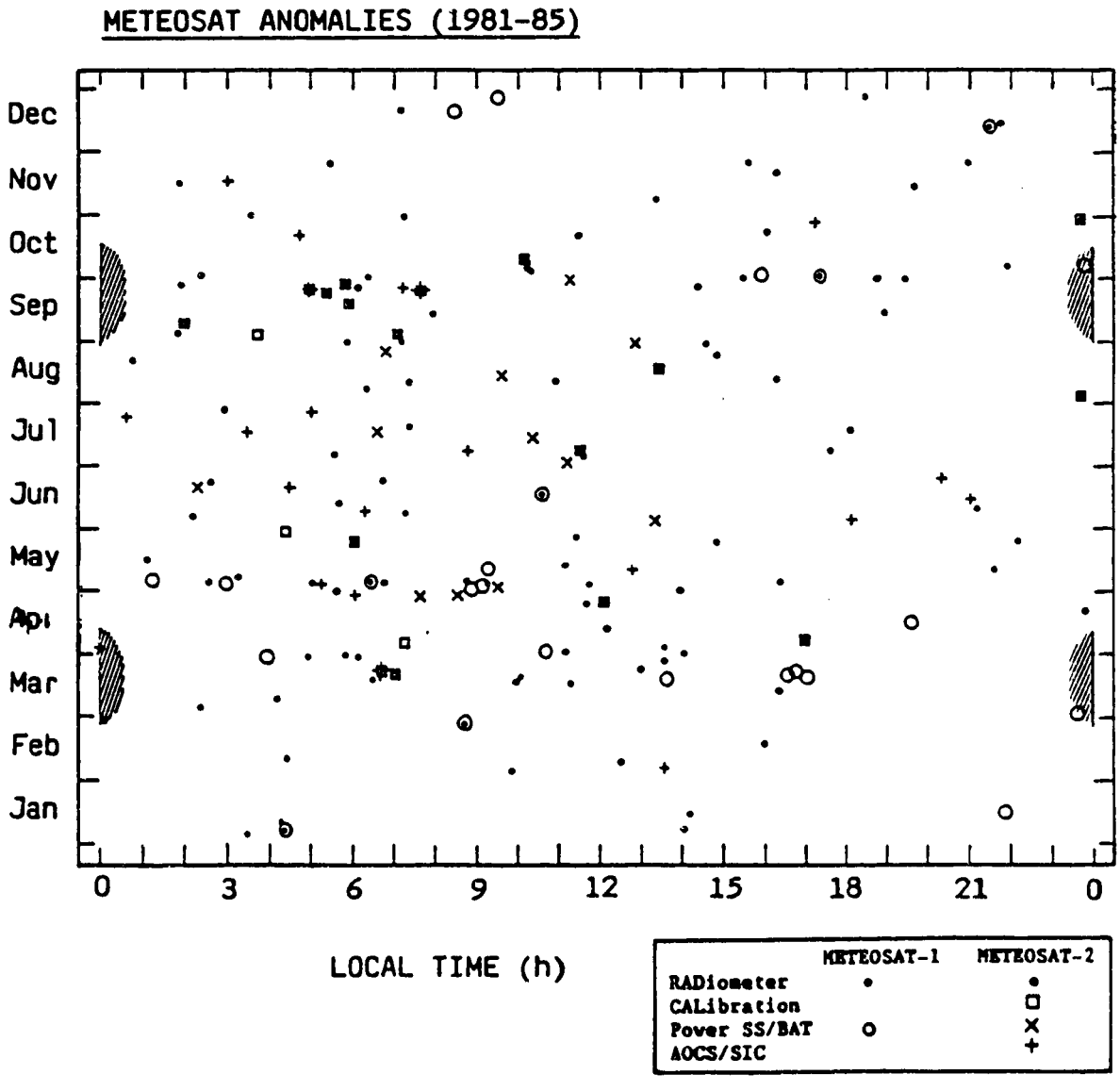
METEOSAT ANOMALIES (1981-85)
Dec
Nov
Oct
Sep
Aug
Jul
Jun
May
Apr
Mar
Feb
Jan
0
3
6
9
12
15
18
21
0
LOCAL TIME (h)
METEOSAT-1
METEOSAT-2
RADiometer
CALibration
Power SS/BAT
AOCS/SIC

Figure 3

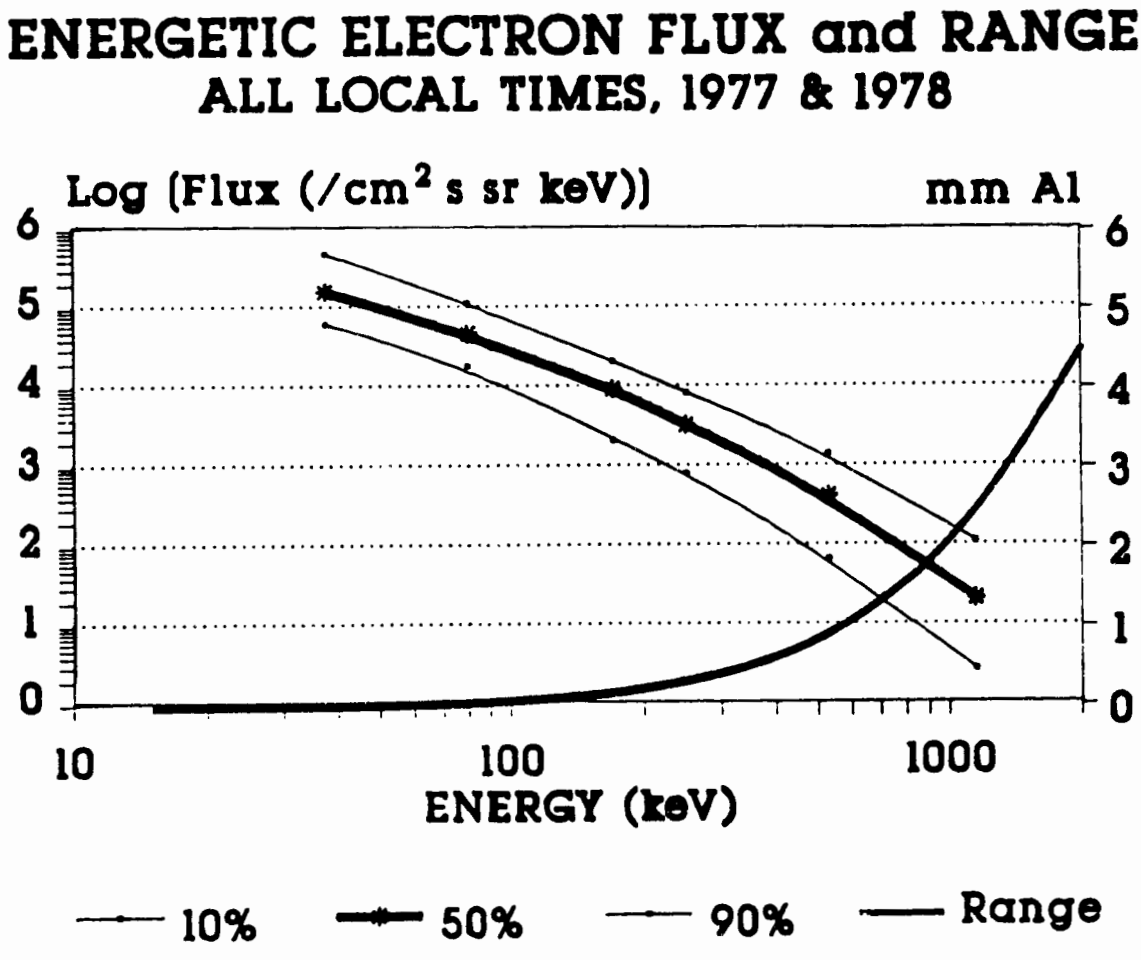
ENERGETIC ELECTRON FLUX and RANGE
ALL LOCAL TIMES, 1977 & 1978
Log (Flux (/cm² s sr keV))
mm Al
6
5
4
3
2
1
0
10
100
1000
ENERGY (keV)
10%
50%
90%
Range

Figure 4

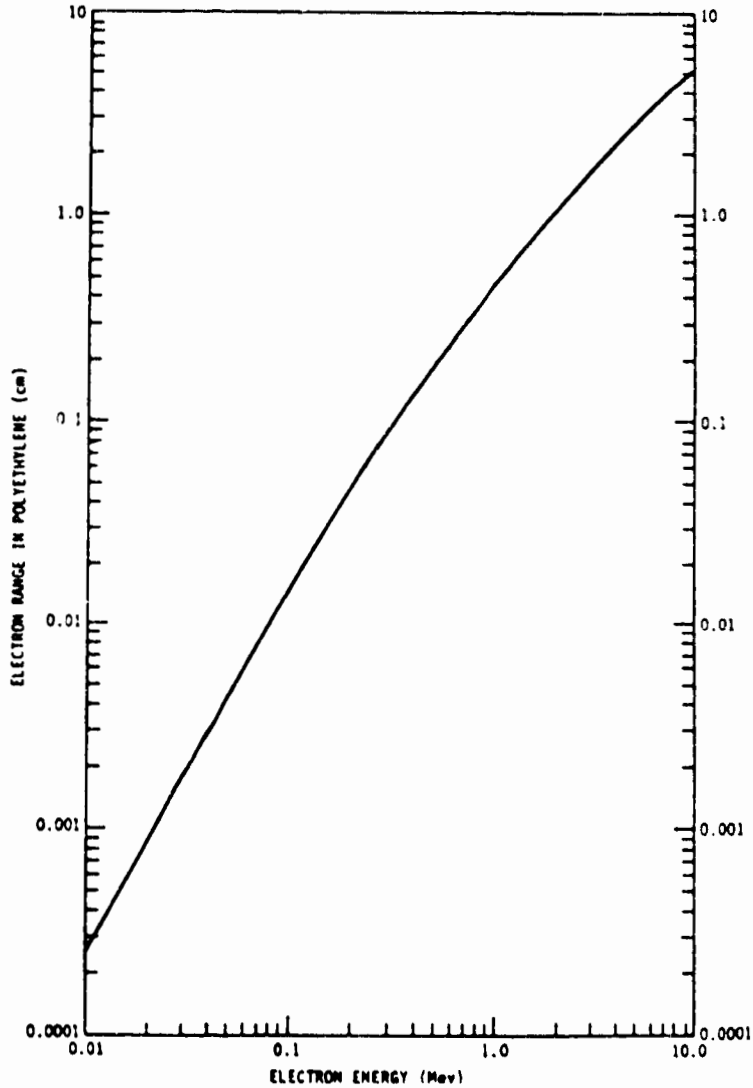
ELECTRON RANGE IN POLYETHYLENE (cm)
10
1.0
0.1
0.01
0.001
0.0001
0.01
0.1
1.0
10.0
ELECTRON ENERGY (Mev)

Figure 5

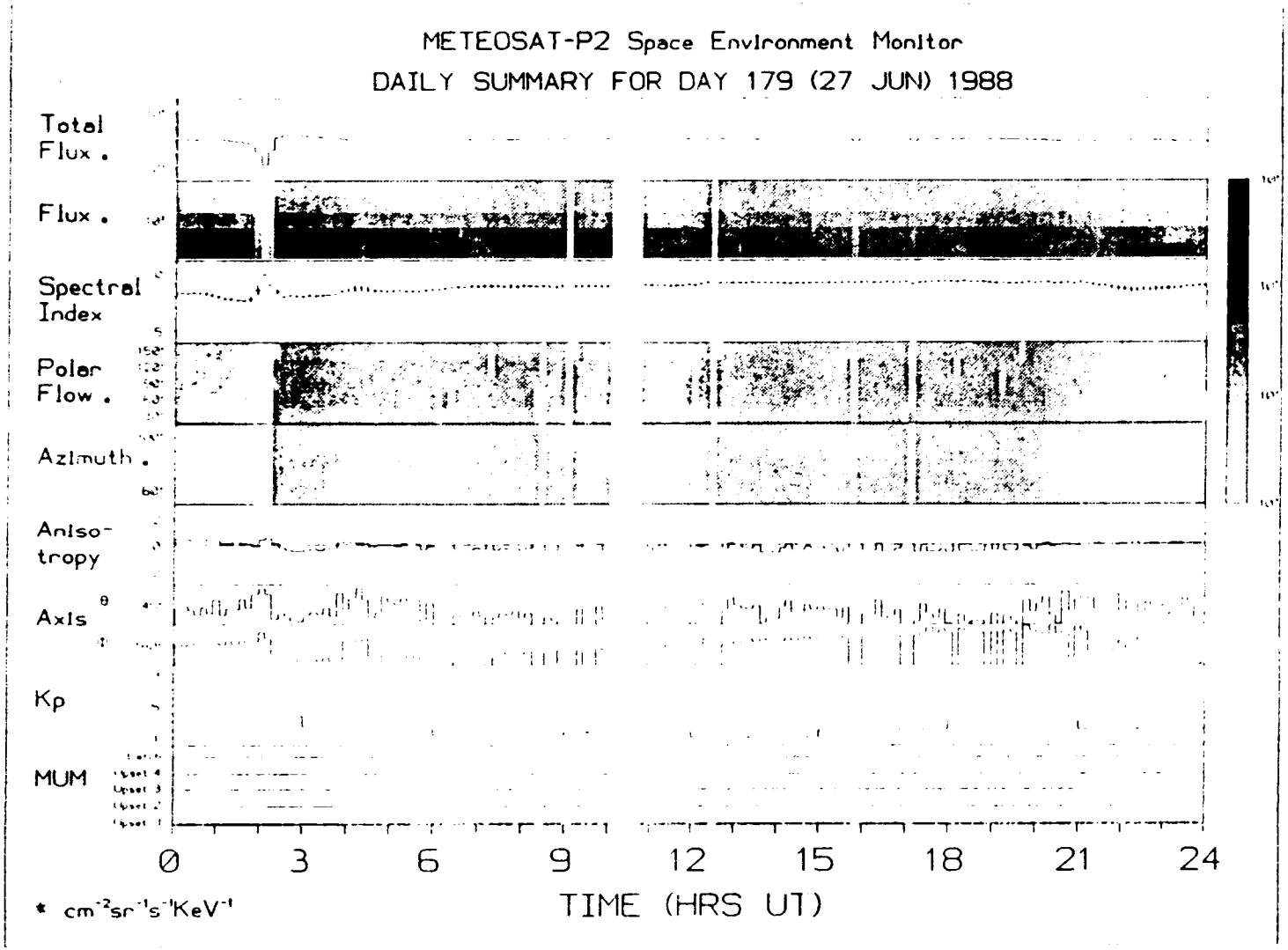
METEOSAT-P2 Space Environment Monitor
DAILY SUMMARY FOR DAY 179 (27 JUN) 1988
Total Flux .
Flux .
Spectral Index
Polar Flow .
Azimuth .
Aniso-tropy
Axis
Kp
MUM
0
3
6
9
12
15
18
21
24
TIME (HRS UT)
* cm⁻²sr⁻¹s⁻¹KeV⁻¹

Figure 6

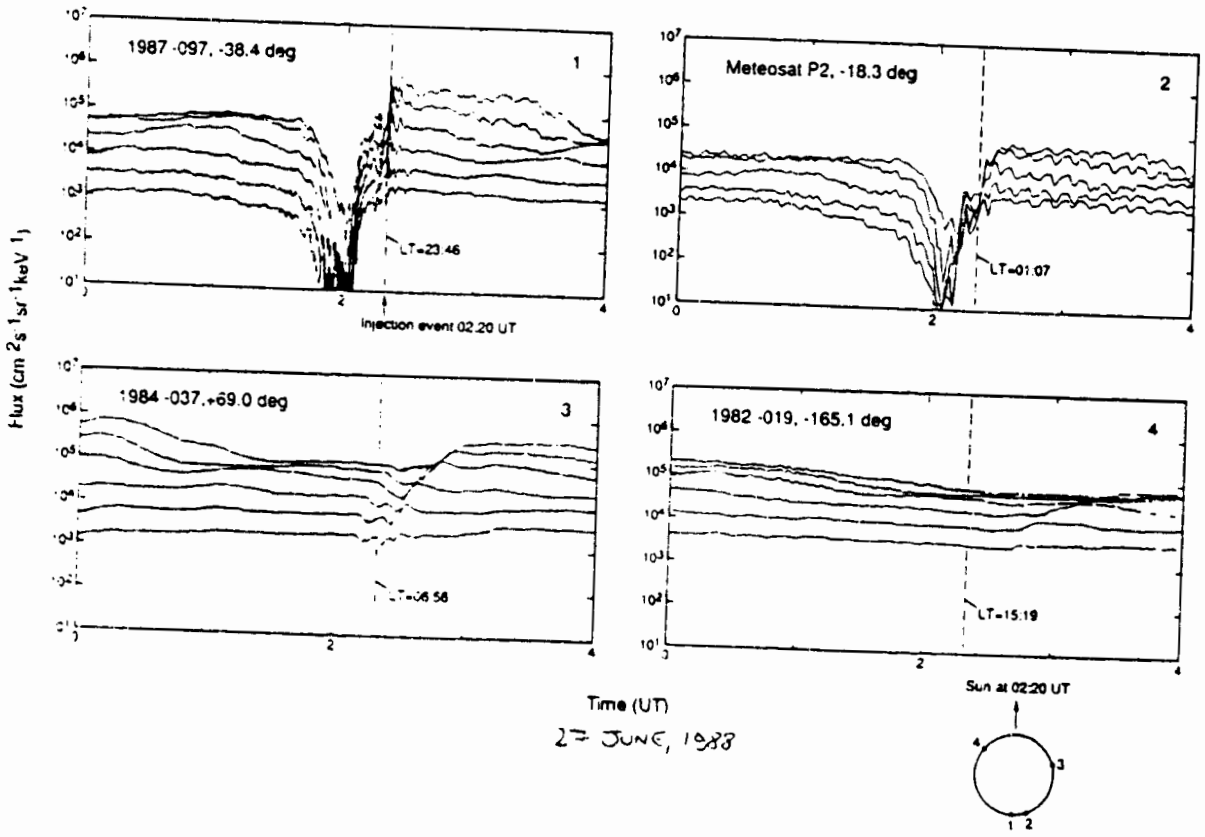
1987 -097, -38.4 deg
1
LT=23:46
Injection event 02:20 UT
Meteosat P2, -18.3 deg
2
LT=01:07
1984 -037, +69.0 deg
3
LT=06:56
1982 -019, -165.1 deg
4
LT=15:19
Flux (cm 2s 1sr 1keV 1)
Time (UT)
27 JUNE, 1988
Sun at 02:20 UT
4
3
1 2

Figure 7

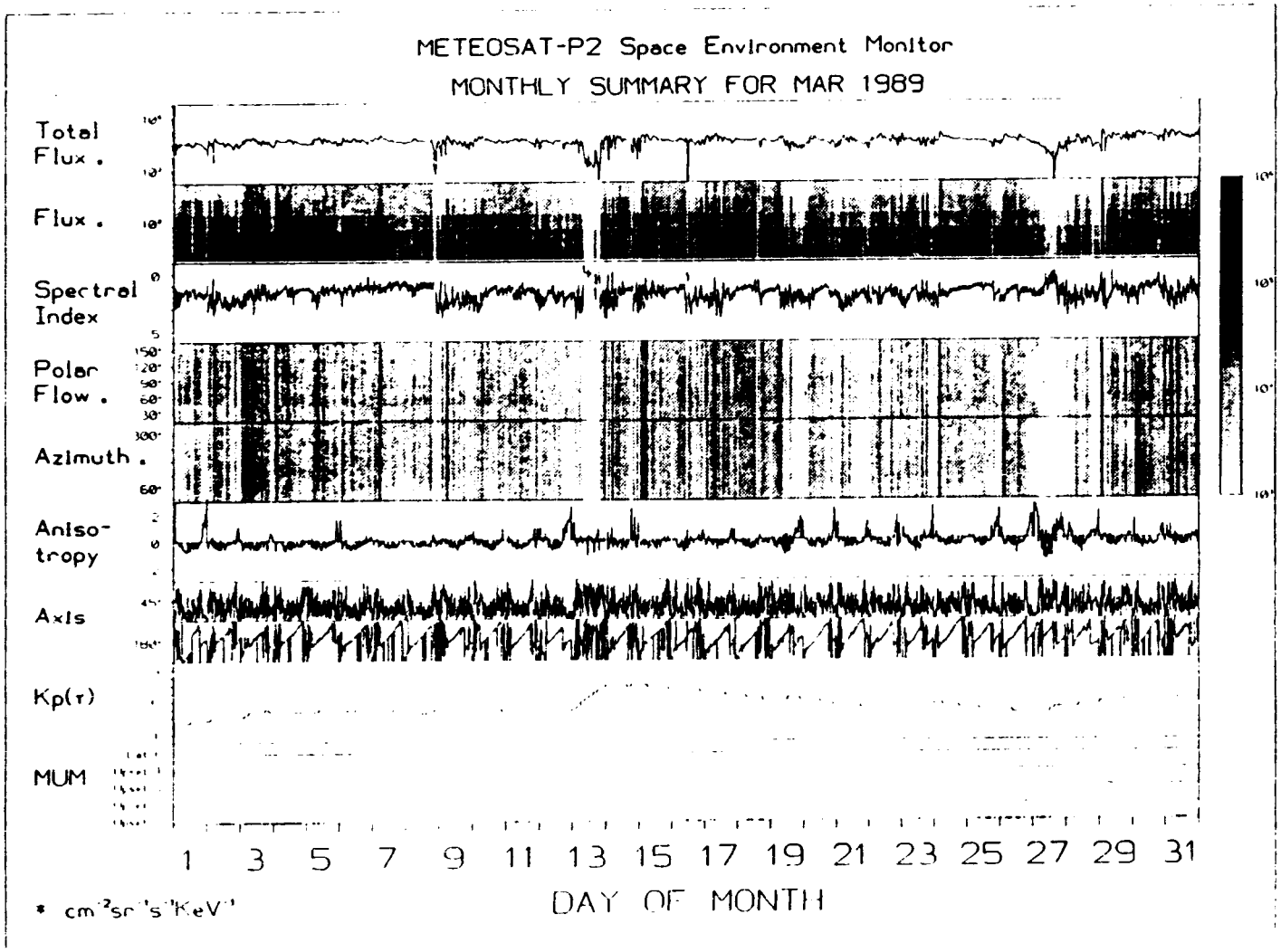
METEOSAT-P2 Space Environment Monitor
MONTHLY SUMMARY FOR MAR 1989
Total Flux .
Flux .
Spectral Index
Polar Flow .
Azimuth .
Aniso-tropy
Axis
Kp(r)
MUM
1 3 5 7 9 11 13 15 17 19 21 23 25 27 29 31
DAY OF MONTH
* cm⁻²sr⁻¹s⁻¹KeV⁻¹

Figure 8

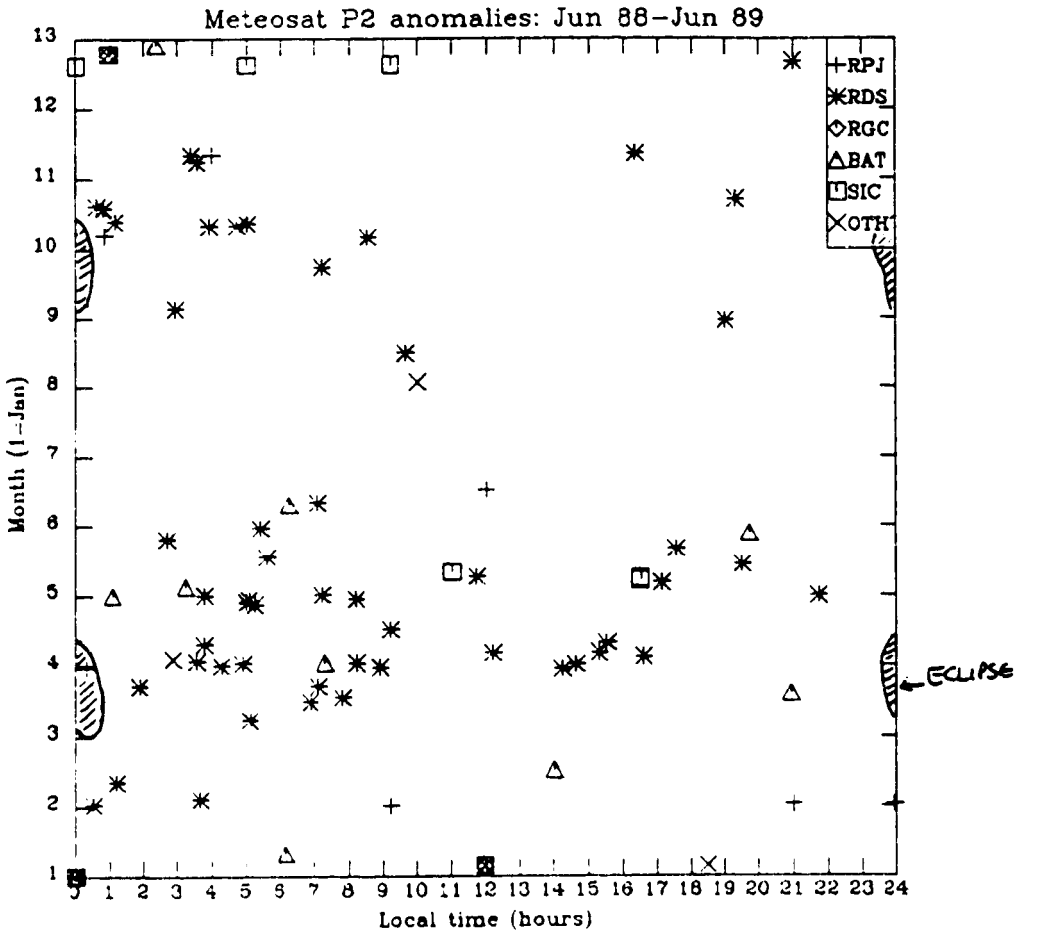
Meteosat P2 anomalies: Jun 88–Jun 89
Month (1=Jan)
Local time (hours)
RPJ
RDS
RGC
BAT
SIC
OTH
ECLIPSE

Figure 9

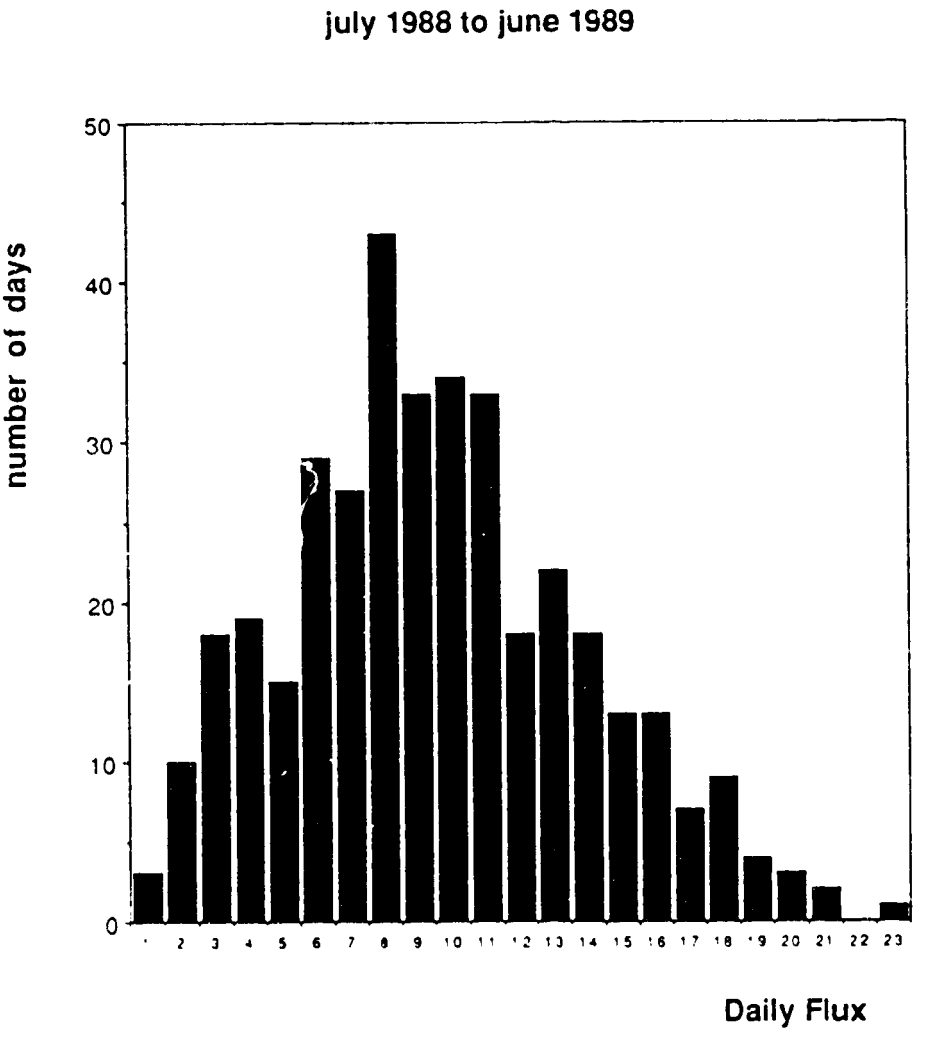
july 1988 to june 1989
number of days
50
40
30
20
10
0
1 2 3 4 5 6 7 8 9 10 11 12 13 14 15 16 17 18 19 20 21 22 23
Daily Flux

FIGURE 10

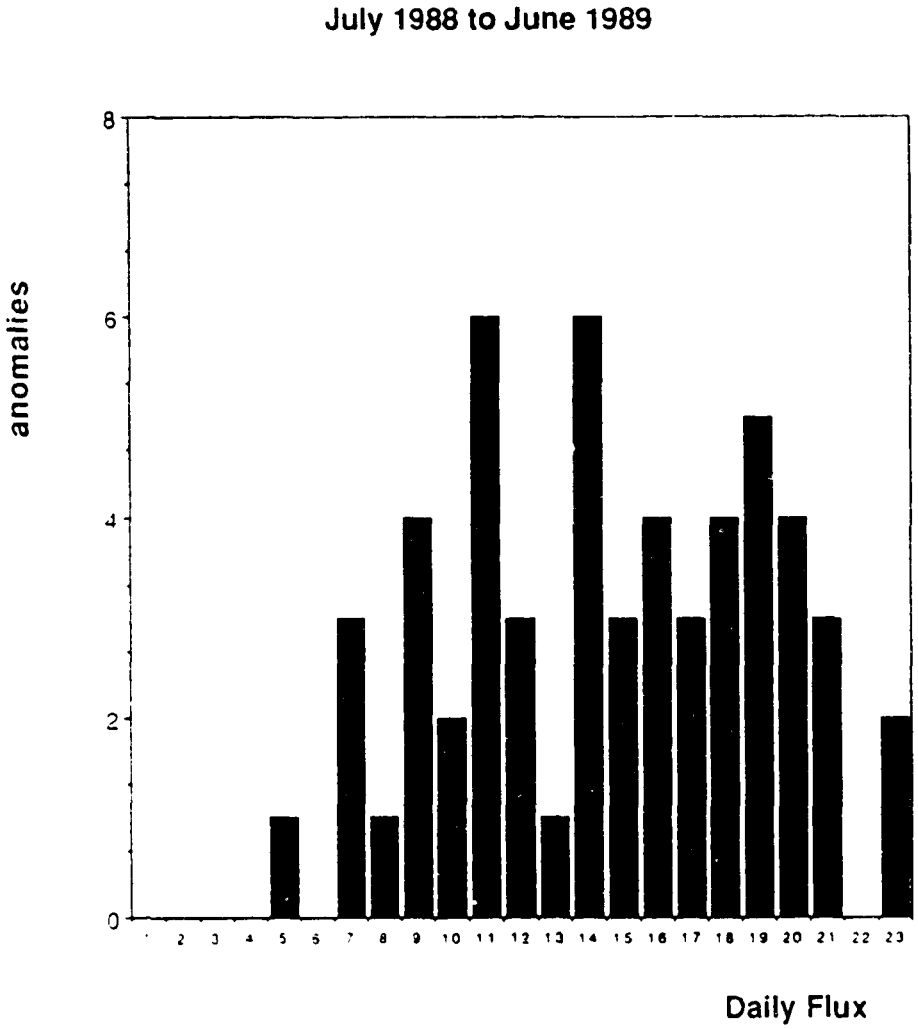
July 1988 to June 1989
anomalies
8
6
4
2
0
1 2 3 4 5 6 7 8 9 10 11 12 13 14 15 16 17 18 19 20 21 22 23
Daily Flux

Figure 11

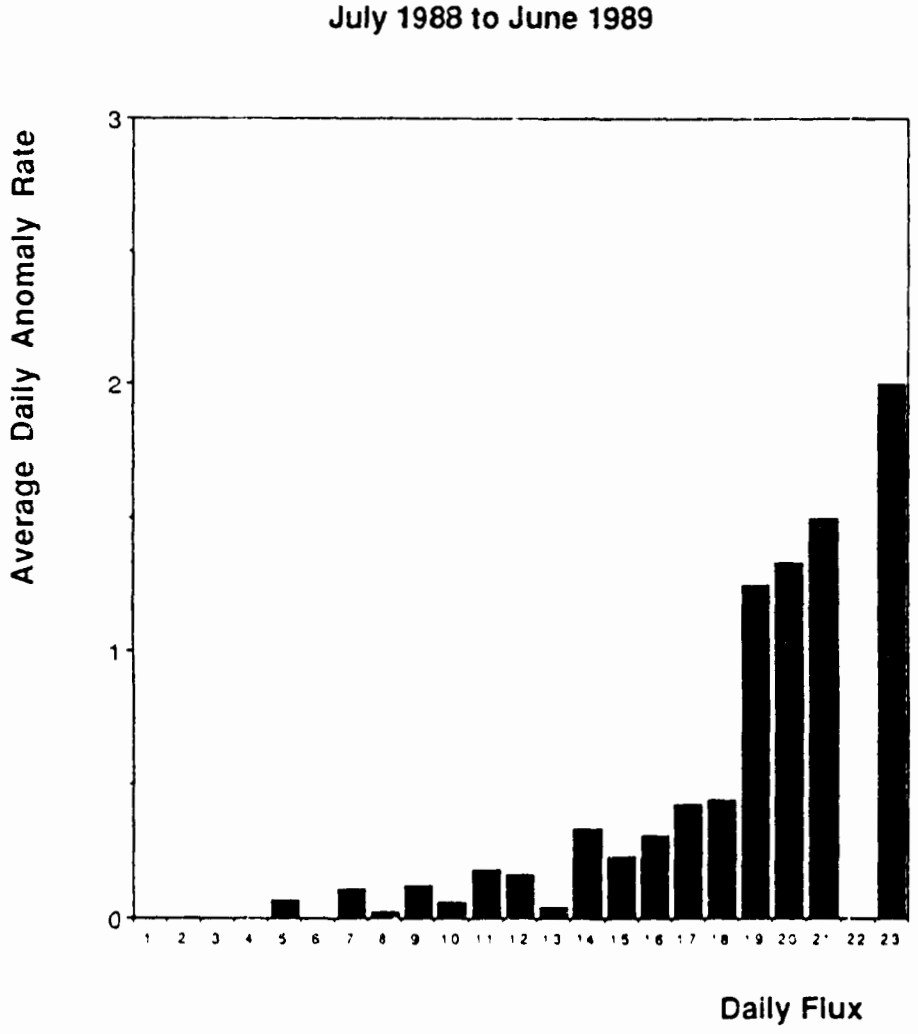
July 1988 to June 1989
Average Daily Anomaly Rate
3
2
1
0
1 2 3 4 5 6 7 8 9 10 11 12 13 14 15 16 17 18 19 20 21 22 23
Daily Flux

Figure 12

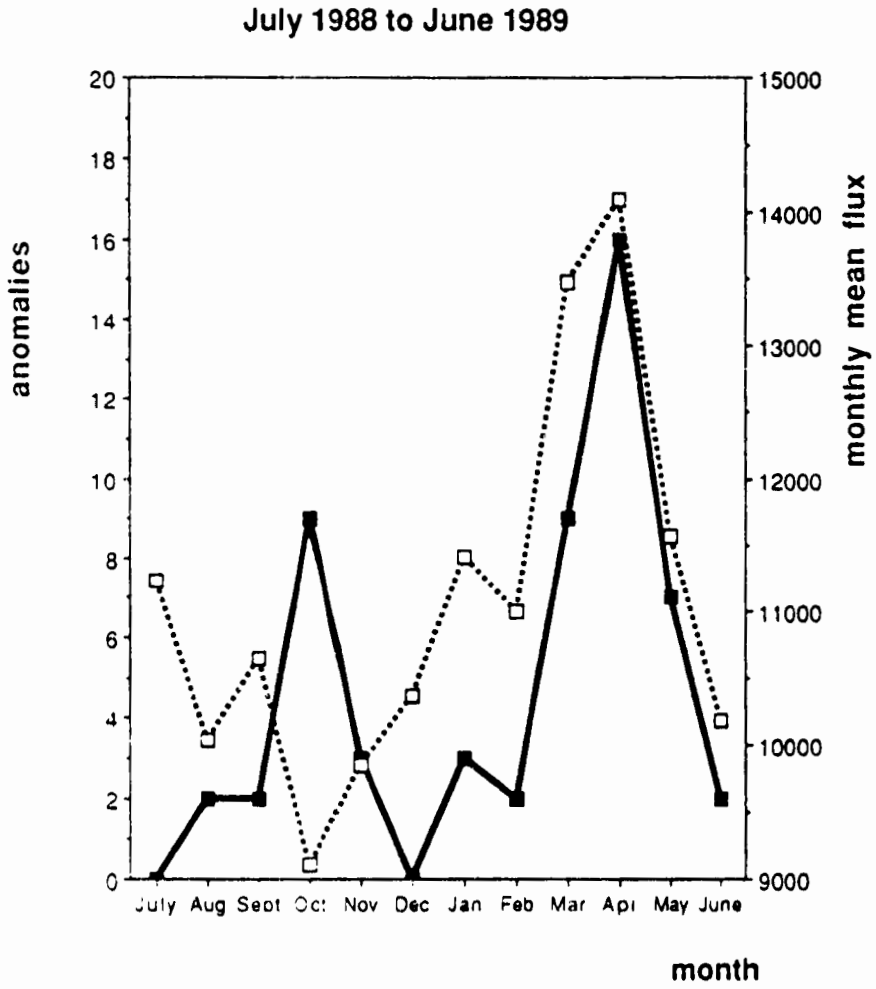
July 1988 to June 1989
anomalies
monthly mean flux
month
20
18
16
14
12
10
8
6
4
2
0
15000
14000
13000
12000
11000
10000
9000
July Aug Sept Oct Nov Dec Jan Feb Mar Apr May June

Figure 13